HHS Public Access

Author manuscript

Radiol Clin North Am. Author manuscript; available in PMC 2017 September 21.

Published in final edited form as:

Radiol Clin North Am. 2017 March ; 55(2): 243–258. doi:10.1016/j.rcl.2016.10.003.

Imaging of Solid Renal Masses

Fernando U. Kay, MD[a] and **Ivan Pedrosa, MD**[b]

[a]Department of Radiology, UT Southwestern Medical Center, Harry Hines 5323, 2201 Inwood Road, Dallas, TX 75390, USA

[b]Department of Radiology and Advanced Imaging Research Center, UT Southwestern Medical Center, Harry Hines 5323, 2201 Inwood Road, Dallas, TX 75390, USA

Abstract

Detection of solid renal masses has increased in the last decades, although it has not resulted in significant mortality reduction from renal cell carcinoma. Consequently, efforts for improved lesion characterization have been pursued and incorporated in management algorithms, in order to distinguish clinically significant tumors from favorable or benign conditions. Concurrently, imaging methods have built a broad base of evidence supporting their role as useful tools not only in lesion detection, but also characterization. In addition, newer modalities, such as contrast enhanced ultrasound, and advanced applications of magnetic resonance imaging, are being investigated. The purpose of this paper is to review the current role of different imaging methods in the characterization of solid renal masses.

Mesh

Renal cell carcinoma; Lymphoma; Angyomiolipoma; Renal oncocytoma; Ultrasound; X-ray computed tomography; Magnetic resonance imaging; Image-guided biopsy

1) Introduction

The incidence of renal cancer has increased from 7.1 to 10.8 cases per 100,000 patients between 1983 and 2002, with most primary tumors initially diagnosed as incidental small renal masses (i.e., measuring less than or equal to 4 cm) during imaging studies performed for other clinical reasons.[1] Paradoxically, this increased in diagnosis has not been associated with better clinical outcomes, with a reported increase in mortality from 1.5 to 6.5 deaths per 100,000 patients within the same time interval.[2] Furthermore, the majority of incidentally detected tumors will either grow slowly[3] or not show detectable growth over time[4,5]. Therefore, cost-effective imaging strategies are necessary to identify clinically significant renal masses, which could evolve into life-threatening disease, while avoiding the unnecessary morbidity and financial costs associated with overtreatment of benign or favorable malignant conditions.

*Corresponding author: ivan.pedrosa@utsouthwestern.edu.

The first step in the workup of incidentally found renal masses is to differentiate benign cysts from solid masses.[6,7] Solid renal masses contain little or no fluid, and are composed predominantly of vascularized tissue (i.e., elements enhancing with the administration of exogenous contrast agents).[7] Despite its lower prevalence compared to cystic lesions, up to 90% of solid masses are reported malignant.[8–10] The risk of malignancy is influenced by size, occurring in approximately 50% for lesions smaller than 1 cm and more than 90% for masses greater than or equal to 7 cm.[8]

Solid malignant masses most frequently encountered in clinical practice are renal cell carcinoma (RCC), urothelial carcinoma, lymphoma, and metastasis, while the most frequently encountered benign solid renal masses are angiomyolipoma (AML), oncocytoma, and inflammatory pseudotumors/pseudolesions. This article provides a comprehensive comprehensive approach to the imaging findings of common malignant and benign renal masses on state-of-the-art ultrasound (US), computed tomography (CT) and magnetic resonance imaging (MRI), proposing strategies to differentiate benign from malignant lesions, and to distinguish RCC subtypes.

1.1) Malignant Lesions

a) Renal Cell Carcinoma—RCC accounts for 3.7% of all solid malignancies and is more common among men (1.6:1, M:F). Patients with localized disease have 92% 5-year survival, while this decreases to 65% for those with regional metastasis, and 12% for patients with distant metastatic disease.[11]

The World Health Organization classification subdivides RCC in different histological groups[12], with clear cell RCC (ccRCC) accounting for 70 to 75%, papillary RCC (pRCC) for 10 to 21%, and chromophobe RCC (chrRCC) for 5% of all RCC cases[12,13]. Survival heavily depends on staging, histological grade (Furhman/International Society of Urological Pathology, ISUP), presence of sarcomatoid change, and necrosis. In addition, ccRCC is associated with worse prognosis than pRCC and chrRCC.[12,14] Different histolopathologic subtypes have distinct features on imaging studies and these are discussed later.

b) Urothelial Carcinoma—Urothelial carcinoma originates from the epithelium of calyces and renal pelvis and may comprise up to 15% of all renal tumors.[15] Median age at diagnosis is above 60, with approximately 2:1 M/F ratio, and hematuria being the most frequent presentation.[15,16] Synchronous and metachronous involvement of the urinary tract may occur in 24% and 11% of patients with renal urothelial carcinoma, respectively.[17] Differentiation of upper-tract urothelial carcinoma from RCC and other solid renal masses is simpler during earlier stages, when the presentation is characterized by wall thickening of the urothelial tract or filling defects in the collecting system. Infiltrative masses in the renal sinus or parenchyma are features of advanced disease, when distinction from aggressive forms of RCC is difficult.[18]

c) Lymphoma—Lymphomatous involvement of the kidneys is most frequently the result of secondary spread of non-Hodgkin’s disease, with prevalence at autopsy reaching 50% in this population.[19] Renal lymphoma may present as multiple masses, solitary lesions simulating RCC, retroperitoneal/perirenal disease, and infiltrative renal disease. A pattern of

multiple renal masses is encountered in up to 60% of the patients, typically ranging from 1 to 3 cm, with homogenous attenuation (CT) or signal intensity (MRI), and low-level postcontrast enhancement compared to background parenchyma (figure 1). There is associated lymphadenopathy elsewhere in the abdomen in less than 50% of the patients with renal involvement.[20] Solitary lesions occur in 10 to 20% of the patients, and although differentiation from ccRCC is possible due to homogeneous signal/attenuation and low-grade enhancement, biopsy may be needed to discriminate from non-ccRCC subtypes, such as papillary tumors.[21]

d) Metastases—The reported prevalence of metastatic disease to the kidneys in oncological patients differs depending on the method of assessment, varying from 20% on autopsy studies, to less than 1% in clinicopathological studies.[22] Commonly, the primary tumor is already known or diagnosed at the same time as the renal lesion, with more than half of the cases occurring in patients over 60 years.[22] The most common primary sites are lung, breast, female genital tract, head and neck, colon, and prostate. Bilateral or multiple masses are found in 23% and 30% of the patients, respectively.[22] Renal metastases occur more commonly at the junction of the renal cortex and medulla, often exhibiting ill-defined borders and low-level enhancement, except in the case of hypervascular primary tumors (e.g. RCC, thyroid, choriocarcinoma). These features may help to suggest the diagnosis, which differ from the most common well-defined appearance of cortical-based RCCs, although a definitive diagnosis usually requires biopsy.

1.2) Benign Lesions

The reported prevalence of benign renal lesions is 13% to 16% of all surgically resected lesions.[8,10] The likelihood of benign histology in small solid renal masses is influenced by size, with prevalence of up to 40% in lesions less than 1 cm in diameter.[23] AMLs and oncocytomas comprise most of the benign solid masses, representing 44% and 35%, respectively.[1]

a) Angiomyolipoma—AMLs are benign neoplasms, consisting of aberrant blood vessels, smooth muscle, and mature adipose tissue[2], representing 2% to 6% of all resected tumors in surgical series[3,4]. Most of these neoplasms are found incidentally on imaging (e.g., 0.1–0.2% of US exams), with female preponderance (1:2, M/F).[5] AML can occur sporadically or in association with genetic syndromes. Prevalence in patients with tuberous sclerosis vary from 55% to 90%, and in patients with lymphangioleiomyomatosis from 30% to 50%.[2] Larger AMLs may cause symptoms, and spontaneous hemorrhage (Wunderlich syndrome), which is a life-threatening complication in larger tumors.[6]

The detection of fatty tissue (i.e., adipocytes) by CT or MRI is regarded as the most specific feature for this diagnosis, although many pathologically proven AMLs do not show fatty tissue on imaging, causing a diagnostic challenge.[7] The diagnosis of classic AMLs containing fat and AML with minimal/absent fat is discussed later.

b) Oncocytoma—Oncocytomas are relatively uncommon cortical tumors (approximately 7% of renal masses in surgical series) composed of oncocytes (polygonal or round-shaped

cells, with moderate to abundant granular cytoplasm), surrounded by thin capillaries and stroma.[8] Patients are usually asymptomatic, being more frequently men (1.2:1, M/F), with a mean age of 65 years at diagnosis. Intratumoral hemorrhage and central scars are present in 20% and 33% of all oncocytomas, respectively, and multifocality may occur in 13% of the patients.[8] Although oncocytomas are classified as benign tumors[9], case reports have described malignant potential[10]. Similarly, aggressive local behavior may manifest with intravascular extension into branches of the renal vein[11] and invasion of the perinephric fat, the latter occurring in up to 7% of all oncocytomas[12](figure 2).

c) Inflammatory Conditions and Pseudotumors—A variety of non-neoplastic conditions may mimic solid renal masses. While developmental renal pseudotumors (e.g., prominent columns of Bertin, dromedrary humps, persistent fetal lobulations) are more easily differentiated from true renal masses by characterization of normal renal parenchyma imaging features (e.g. on multiphasic dynamic contrast enhanced imaging), infectious, inflammatory and granulomatous diseases (e.g., pyelonephritis/abscess, xanthogranulomatous pyelonephritis) may pose a significant diagnostic challenge.[13] Interpretation of the imaging findings in the appropriate clinical context is crucial, since focal or multifocal pyelonephritis is usually accompanied by characteristic symptoms, such as chills, fever, flank pain and pyuria. US-Doppler and contrast-enhanced CT or MR may demonstrate single or multiple hypoperfused wedge-shaped areas, extending from the papilla to the cortex.[14] Xantogranulomatous pyelonephritis can also present as renal masses in patients with flank pain and fever, and is more commonly observed in middle-aged women with urinary stones, infection (most common by Escherichia coli and Proteus), and/or congenital anomalies.[15,16] This disease is characterized by destruction of the normal renal architecture, enlarged kidney, contracted pelvis, associated with staghorn calculus, and perinephric inflammatory changes.[14]

2) Imaging Techniques

2.1) Ultrasound

US is generally the first line for patients with suspected renal disease given its lower cost, wide availability, and lack of ionizing radiation. There is no current role for RCC screening with US in the general population. The prevalence of incidental renal masses in asymptomatic persons undergoing US is about 0.4%, with half of the cases resulting in RCC.[17] US is indicated in the evaluation of upper urinary tract symptoms and in the workup of indeterminate renal masses (ACR-Appropriateness Criteria® rating 8)[18]. It has been favored over non-enhanced MRI and CT in patients with contraindications to intravenous contrast, with lower sensitivity in the detection of small-sized lesions in comparison to contrast-enhanced CT[19–21]. US is not indicated to stage renal cancer (ACR-Appropriateness Criteria® rating 3)[22].

Characterization of cystic renal lesions is most frequently straightforward on US, although the appearance of complex cystic masses and solid lesions may overlap. Simple renal cysts are anechoic structures with positive through transmission and refraction along the sidewalls, demonstrating sharp and smooth walls.[23] Cysts with hemorrhagic or proteinaceous contents

may harbor internal echoes or debris. Harmonic imaging can minimize reverberation artifacts related to so-called dirty echoes, facilitating the distinction of cysts from solid masses.[24,25] As with other imaging techniques, the detection of blood flow on Doppler, or lesion enhancement after intravenous contrast injection, are unequivocal evidence of a solid mass.[26]

2.2) Computed Tomography

The most commonly used method to evaluate indeterminate renal masses is contrast-enhanced CT (ACR – Appropriateness Criteria® rating 9).[18] It is also considered the method of choice to stage renal cell carcinoma (ACR – Appropriateness Criteria® rating 9)[22], with high accuracies in both early and advanced stages[27]. A CT protocol for evaluation of renal masses is proposed in Table 1.

The sensitivity of CT for small renal masses is higher than 90%[19], approaching 100% for lesions larger than 2 cm[20]. An advantage of CT over US and MRI is the ability to characterize lesions in Hounsfield units (HU), a quantitative standardized x-ray attenuation scale. Differences of at least 10 HU between pre- and post-contrast CT images have been historically proposed as cutoff values to differentiate solid masses from renal cysts.[28,29] More conservative values, such as 15 to 20 HU are generally used in clinical practice to account for volume averaging artifacts and misregistration among acquisitions[30]. The average attenuation of renal lesions larger than 1 cm on non-enhanced CT scans is also useful in their characterization: values less than 20 HU or more than 70 HU are associated with simple and hemorrhagic/proteinaceous cysts, respectively.[31]

The last decade witnessed the emergence of dual-energy CT (DECT) as a promising technique to evaluate renal masses, with increased specificity in the detection of post-contrast enhancement, and the potential role to reduce radiation dose.[32]

2.3) Magnetic Resonance Imaging

MRI is indicated in the evaluation of indeterminate renal masses and staging of renal cancer (ACR-Appropriateness Criteria® rating 8), usually favored over contrast-enhanced CT in patients with moderate chronic kidney disease (CKD) (i.e., estimated glomerular filtration rate, eGFR between 30 and 60 mL/min/1.73m^2).[18] Recently, the safety of newer gadolinium-based contrast agents (e.g. macrocyclic), even in patients with stages 4 and 5 CKD (eGFR < 30 mL/min/1.73m^2), has been advocated based on the absence of new cases of nephrogenic systemic fibrosis observed in large cohorts of patients.[33,34] In addition, non-enhanced sequences, such as arterial spin labeling (ASL), may aid in the evaluation of vascularity in renal masses.[35] Perfusion parameters obtained by ASL are correlated with those obtained by dynamic contrast-enhanced MRI, as well as with vessel density in renal tumors.[36]

MR imaging is particularly helpful to distinguish solid from cystic lesions when enhancement of renal masses is questionable on CT, especially for those with net-enhancement between 10 and 20 HU.[37] In addition, diffusion weighted imaging (DWI) and dynamic contrast-enhanced (DCE) MRI can provide specific information regarding the

tumor histology.[38] As discussed later, the use of those parameters may help to differentiate benign from malignant renal masses, the RCC subtype, and predict tumor grade.

An MR imaging protocol for evaluation of renal masses is provided in Table 2. Images are acquired in end expiration to improve consistency of kidney position between scans, with patient's arms located above the head, when possible, to avoid phase-wrap artifacts.[39]

3) Impact of Imaging Methods on Patient Management

Increased detection rates and lower intrinsic prevalence of malignancy in small renal masses has generated a challenging situation in patient management. Mainstream treatment of renal cancer is still surgical, as nephron sparing techniques achieves similar oncological results when compared to radical nephrectomy in small RCC.[40,41] However, subgroups of patients such as the elderly, those with multiple comorbidities, and those with favorable tumor histology, may benefit from conservative approaches such as active surveillance.[42,43] Current strategies propose the utilization of size, histologic subtype, nuclear grade, and clinical criteria as parameters for the decision between active surveillance or surgical treatment.[44]

3.1) Diagnosis of Benign Disease

The ability to distinguish benign from malignant solid renal masses by US is limited.[45] Even the classic appearance of AML on US as hyperechoic masses is not specific, overlapping with RCC features.[46–48] However, contrast-enhanced US (CEUS) is a promising modality, which can potentially add value in the characterization of renal masses. In a large cohort of patients, CEUS performed with a sensitivity of 100% and specificity of 95% in the diagnosis of malignancy among cystic and solid indeterminate renal masses.[49]

Unequivocal demonstration of bulk fat (i.e., adipocytes) by CT or MRI in a renal lesion is a specific finding for the diagnosis of AML[50,51]. On unenhanced CT, determination of macroscopic fat is achieved when values less than −10 HU are obtained (figure 3).[52] On MR imaging, bulk fat follows the signal intensity of subcutaneous and intraabdominal fat on all sequences, characterized by: 1) hyperintense signal on T1- or T2-weighted images, with signal saturation after frequency selective fat-saturation technique; 2) high signal intensity on T1-weighted "in-phase" (IP) and "opposed-phased" (OP) imaging, with signal dropout on OP at the interface of the lesion with the kidney ("India-ink artifact"); 3) high signal intensity on "fat-only" reconstructions from Dixon-based acquisitions[53](figure 4). Coexistence of areas of both bulk and intravoxel fat (scant amounts of fat mixed with smooth-muscle and vessels), the latter manifested as areas of decreased signal on OP images compared to IP images, are common in AML.[54]

Some AMLs may not show bulk fat on imaging (AML with minimal fat, mfAML)[55], whereas signal loss on OP images is also commonly present in ccRCC, given the presence of intracytoplasmic lipid-containing vacuoles[56,57]. Therefore, in the authors' experience, the isolated presence of decreased signal on OP imaging relative to IP imaging is not useful in the differentiation of ccRCC from mfAML in small renal masses.[58] The diagnosis of mfAML should be considered for renal masses with homogeneous low-signal intensity

relative to renal cortex on T2-weighted images, particularly for smaller lesions found in women, in the absence of bulk fat, plus or minus minimal amount of fat (i.e. decreased signal intensity on OP imaging).[58] In contrast, the presence of intratumoral necrosis and cystic changes favor ccRCC over mfAML.[58] In addition, a simplified perfusion parameter, known as arterial/delay enhancement ratio, and defined as the difference in signal intensity between arterial and pre contrast phase divided by the difference between delayed and pre contrast phase, has been proposed to distinguish mfAML from RCC, with values greater than 1.5 favoring the first.[59] Ultimately, the combination of multiple MR imaging parameters may provide better diagnostic performances, with up to 100% sensitivity and 89% specificity for the diagnosis of mfAML (figure 5).[60]

DWI can provide surrogate information about cellular density, and can potentially assist in the differentiation of benign and malignant lesions. A meta-analysis reported significantly lower apparent diffusion coefficients (ADCs) in RCC, with 95% confidence intervals ranging from 1.45 to 1.77×10^{-3} mm^2/s, while values obtained from benign lesions ranged between 1.92 and 2.28×10^{-3} mm^2/s. Particularly, oncocytomas had significantly higher ADC values than malignant lesions, ranging from 1.84 to 2.17×10^{-3} mm^2/s, while this was not observed for AML, with values between 1.25 and 1.83×10^{-3} mm^2/s.[61]

Segmental enhancement inversion, a radiologic sign defined as the presence of a heterogeneous pattern of postcontrast enhancement on corticomedullary phase that inverts on early excretory phase, was initially reported to have 80% sensitivity and 99% specificity to distinguish oncocytomas from RCC.[62] However, a more recent study comparing oncocytomas and chrRCC did not show significant differences in the prevalence of segmental enhancement inversion sign between entities.[63] Higher ASL perfusion levels were reported in oncocytomas compared to clear cell and non-clear cell subtypes of RCC[64], although some overlap is present.

3.2) Characterization of RCC Subtypes

Attempts to histologically subtype RCCs on Doppler or CEUS have been inconsistent so far.[65] On CT, differentiation of RCC subtypes generally relies on analyses of post-contrast time-attenuation curves and lesion homogeneity. Postcontrast enhancement of ccRCC is significantly higher than that observed for pRCC and chRCC, while heterogeneity is also more frequently seen in ccRCC histology (figure 6).[66–68]

Relative ratios of renal mass enhancement to enhancement of the aorta are significantly lower for pRCC than for non-papillary histology on CT, with sensitivity and specificity of 86% and 85%, respectively, using a cutoff of 0.25.[69] Relative enhancement ratios in the renal mass compared to the renal parenchyma are also significantly higher for ccRCC than for pRCC (figure 7).[70]

The MRI phenotype of papillary neoplasms is variable as these tumors evolve from solid hypoenhancing homogeneous masses with low signal intensity on T2-weighted images to more heterogeneous tumors after intralesional hemorrhage. Not infrequently, pRCC presents as hemorrhagic cystic masses with peripheral enhancing components, contained by a well-developed tumor capsule.[57] Regardless of the MRI phenotype, the viable, vascularize

portions of the tumor usually exhibits homogenous low signal intensity on T2-weighted images and low-level enhancement (figure 8).[71,72]

Papillary tumors are further subdivided into type 1 (basophilic, usually low-grade) and type 2 (eosinophilic, usually high-grade) groups, the latter with worse prognosis.[73] Distinction between these two types by imaging is in general not possible for those tumors presenting as localized renal masses, albeit Type 2 tumors tend to be larger.[74] A subgroup of Type 2 papillary RCC can present as ill-defined, invasive tumors, commonly with centripetal growth and renal vein invasion, complicated by pulmonary embolism.[75] The latter imaging phenotype is associated with sensibly worse prognosis than that of well-defined pRCC.[74]

Three-point time-intensity curve analyses have also demonstrated value RCC subtyping. ccRCC has significantly greater signal intensity change (difference between postcontrast and precontrast, divided by precontrast signal intensity) on both corticomedullary and nephrographic phases (205.6% and 247.1%, respectively) compared to pRCC (32.1% and 96.6%), whereas chrRCC has intermediate enhancement values (109.9% and 192.5%) (figure 9). Distinction of ccRCC from pRCC was achieved with high sensitivity and specificity using 84% signal intensity change as the threshold on corticomedullary acquisitions.[76] Perfusion in pRCC by ASL is also lower than perfusion levels observed for ccRCC, chRCC, unclassified RCC, and oncocytoma.[64]

DWI is currently not widely accepted as a tool for subtyping of RCC. A meta-analysis of DWI studies did not demonstrate differences in ADC values among RCC subtypes.[77] Figure 10 summarizes a diagnostic algorithm used by the authors for the categorization of solid renal masses on MR imaging. Note that in those groups indicated with an asterisk, the MR imaging findings of different histologic subtypes can overlap and even with the use of ancillary findings (e.g. homogeneity, necrosis, scar, etc.) a more specific diagnosis may not be possible.

3.3) Characterization of Histological Grade

Tumor histological grade has prognostic implications and therefore may affect patient management. However, the accuracy in pre-surgical grade prediction has been limited for both imaging methods and even percutaneous biopsy. On MR imaging, multivariate models taking into consideration morphologic features of RCC showed that renal vein thrombosis and retroperitoneal collaterals were predictive of high-grade ccRCC, while peripheral location and homogeneous enhancement were associated with low-grade pRCC.[57] DWI may aid in the differentiation of low- from high-grade ccRCC, with sensitivities between 65% and 90%, specificities between 71% and 83%, and overall accuracy of 0.83.[77]

3.4) Imaging-guided Biopsy

Percutaneous renal biopsy has been shown to help avoiding surgery in up to 33% of the cases initially considered to be malignant on imaging.[78] Renal biopsy demonstrated high sensitivity and specificity in identifying malignancy[44,78,79], although the number of non-diagnostic samples may vary between 9%[44] and 29%[78,80]. Considering only diagnostic samples, biopsy of small renal masses has shown up to 94% accuracy in defining histology[44], with lower accuracies to determine Fuhrman grade (46 to 85%)[81]. Severe

complications are rare, occurring in less than 1%[81], leading some to advocate for the incorporation of imaging-guided biopsy into management algorithms of small renal masses[44].

Summary

The continued evolution of imaging methods and evolving management options have bolstered the noninvasive assessment of solid renal masses. The combination of multiple subjective and objective (quantitative) parameters obtained from imaging studies offers an opportunity for evaluating the biology and ultimately the clinical significance of solid renal masses. As a result, patient management may be positively impacted with the use of cutting-edge imaging protocols, along with the development of evidence-based diagnostic algorithms that integrate these novel imaging criteria and percutaneous biopsies.

References

1. Kutikov A, Fossett LK, Ramchandani P, et al. Incidence of benign pathologic findings at partial nephrectomy for solitary renal mass presumed to be renal cell carcinoma on preoperative imaging. Urology. 2006; 68(4):737–740. [PubMed: 17070344]
2. Flum AS, Hamoui N, Said MA, et al. Update on the Diagnosis and Management of Renal Angiomyolipoma. J Urol. 2015
3. Fujii Y, Komai Y, Saito K, et al. Incidence of benign pathologic lesions at partial nephrectomy for presumed RCC renal masses: Japanese dual-center experience with 176 consecutive patients. Urology. 2008; 72(3):598–602. [PubMed: 18649929]
4. Milner J, McNeil B, Alioto J, et al. Fat poor renal angiomyolipoma: patient, computerized tomography and histological findings. J Urol. 2006; 176(3):905–909. [PubMed: 16890650]
5. Fujii Y, Ajima J, Oka K, Tosaka A, Takehara Y. Benign renal tumors detected among healthy adults by abdominal ultrasonography. Eur Urol. 1995; 27(2):124–127. [PubMed: 7744154]
6. Chronopoulos PN, Kaisidis GN, Vaiopoulos CK, et al. Spontaneous rupture of a giant renal angiomyolipoma-Wunderlich's syndrome: Report of a case. Int J Surg Case Rep. 2016; 19:140–143. [PubMed: 26764888]
7. Lane BR, Aydin H, Danforth TL, et al. Clinical correlates of renal angiomyolipoma subtypes in 209 patients: Classic, fat poor, tuberous sclerosis associated and epithelioid. Journal of Urology. 2008; 180(3):836–843. [PubMed: 18635231]
8. PerezOrdonez B, Hamed G, Campbell S, et al. Renal oncocytoma: A clinicopathologic study of 70 cases. American Journal of Surgical Pathology. 1997; 21(8):871–883. [PubMed: 9255250]
*9. Lopez-Beltran A, Scarpelli M, Montironi R, Kirkali Z. 2004 WHO classification of the renal tumors of the adults. Eur Urol. 2006; 49(5):798–805. [PubMed: 16442207]
10. Oxley JD, Sullivan J, Mitchelmore A, Gillatt DA. Metastatic renal oncocytoma. Journal of Clinical Pathology. 2007; 60(6):720–722. [PubMed: 17557872]
11. Hes O, Michal M, Sima R, et al. Renal oncocytoma with and without intravascular extension into the branches of renal vein have the same morphological, immunohistochemical, and genetic features. Virchows Arch. 2008; 452(2):193–200. [PubMed: 18066590]
12. Gudbjartsson T, Hardarson S, Petursdottir V, Thoroddsen A, Magnusson J, Einarsson GV. Renal oncocytoma: a clinicopathological analysis of 45 consecutive cases. BJU Int. 2005; 96(9):1275–1279. [PubMed: 16287444]
13. Bhatt S, MacLennan G, Dogra V. Renal pseudotumors. AJR Am J Roentgenol. 2007; 188(5):1380–1387. [PubMed: 17449786]
14. Craig WD, Wagner BJ, Travis MD. Pyelonephritis: radiologic-pathologic review. Radiographics. 2008; 28(1):255–277. quiz 327–258. [PubMed: 18203942]

15. Chuang CK, Lai MK, Chang PL, et al. Xanthogranulomatous pyelonephritis: experience in 36 cases. J Urol. 1992; 147(2):333–336. [PubMed: 1732587]
16. Osca JM, Peiro MJ, Rodrigo M, Martinez-Jabaloyas JM, Jimenez-Cruz JF. Focal xanthogranulomatous pyelonephritis: partial nephrectomy as definitive treatment. Eur Urol. 1997; 32(3):375–379. [PubMed: 9358230]
17. Haliloglu AH, Gulpinar O, Ozden E, Beduk Y. Urinary ultrasonography in screening incidental renal cell carcinoma: is it obligatory? Int Urol Nephrol. 2011; 43(3):687–690. [PubMed: 20848193]
18. Heilbrun ME, Casalino DD, Beland MD, et al. ACR Appropriateness Criteria® - Indeterminate Renal Mass. 2014
19. Warshauer DM, McCarthy SM, Street L, et al. Detection of renal masses: sensitivities and specificities of excretory urography/linear tomography, US, and CT. Radiology. 1988; 169(2):363–365. [PubMed: 3051112]
20. Jamis-Dow CA, Choyke PL, Jennings SB, Linehan WM, Thakore KN, Walther MM. Small (< or = 3-cm) renal masses: detection with CT versus US and pathologic correlation. Radiology. 1996; 198(3):785–788. [PubMed: 8628872]
21. Kang SK, Chandarana H. Contemporary imaging of the renal mass. Urol Clin North Am. 2012; 39(2):161–170. vi. [PubMed: 22487759]
22. Blaufox MD, Moreno CC, Gore JL, et al. ACR Appropriateness Criteria® - Renal Cell Carcinoma Staging. 2015
23. Hartman DS, Choyke PL, Hartman MS. From the RSNA refresher courses: a practical approach to the cystic renal mass. Radiographics. 2004; 24(Suppl 1):S101–115. [PubMed: 15486234]
24. Desser TS, Jeffrey RB. Tissue harmonic imaging techniques: physical principles and clinical applications. Semin Ultrasound CT MR. 2001; 22(1):1–10. [PubMed: 11300583]
25. Schmidt T, Hohl C, Haage P, et al. Diagnostic accuracy of phase-inversion tissue harmonic imaging versus fundamental B-mode sonography in the evaluation of focal lesions of the kidney. AJR Am J Roentgenol. 2003; 180(6):1639–1647. [PubMed: 12760935]
26. Quaia E. Microbubble ultrasound contrast agents: an update. Eur Radiol. 2007; 17(8):1995–2008. [PubMed: 17351779]
27. Catalano C, Fraioli F, Laghi A, et al. High-resolution multidetector CT in the preoperative evaluation of patients with renal cell carcinoma. AJR Am J Roentgenol. 2003; 180(5):1271–1277. [PubMed: 12704036]
28. Bosniak MA. The small (less than or equal to 3.0 cm) renal parenchymal tumor: detection, diagnosis, and controversies. Radiology. 1991; 179(2):307–317. [PubMed: 2014269]
29. Silverman SG, Lee BY, Seltzer SE, Bloom DA, Corless CL, Adams DF. Small (< or = 3 cm) renal masses: correlation of spiral CT features and pathologic findings. AJR Am J Roentgenol. 1994; 163(3):597–605. [PubMed: 8079852]
30. Maki DD, Birnbaum BA, Chakraborty DP, Jacobs JE, Carvalho BM, Herman GT. Renal cyst pseudoenhancement: beam-hardening effects on CT numbers. Radiology. 1999; 213(2):468–472. [PubMed: 10551228]
31. Pooler BD, Pickhardt PJ, O'Connor SD, Bruce RJ, Patel SR, Nakada SY. Renal cell carcinoma: attenuation values on unenhanced CT. AJR Am J Roentgenol. 2012; 198(5):1115–1120. [PubMed: 22528901]
32. Mileto A, Nelson RC, Paulson EK, Marin D. Dual-Energy MDCT for Imaging the Renal Mass. AJR Am J Roentgenol. 2015; 204(6):W640–647. [PubMed: 25730444]
33. Nandwana SB, Moreno CC, Osipow MT, Sekhar A, Cox KL. Gadobenate Dimeglumine Administration and Nephrogenic Systemic Fibrosis: Is There a Real Risk in Patients with Impaired Renal Function? Radiology. 2015; 276(3):741–747. [PubMed: 25875973]
34. Soulez G, Bloomgarden DC, Rofsky NM, et al. Prospective Cohort Study of Nephrogenic Systemic Fibrosis in Patients With Stage 3–5 Chronic Kidney Disease Undergoing MRI With Injected Gadobenate Dimeglumine or Gadoteridol. AJR Am J Roentgenol. 2015; 205(3):469–478. [PubMed: 26295633]

35. Pedrosa I, Rafatzand K, Robson P, et al. Arterial spin labeling MR imaging for characterisation of renal masses in patients with impaired renal function: initial experience. Eur Radiol. 2012; 22(2): 484–492. [PubMed: 21877173]
36. Zhang Y, Kapur P, Yuan Q, et al. Tumor Vascularity in Renal Masses: Correlation of Arterial Spin-Labeled and Dynamic Contrast-Enhanced Magnetic Resonance Imaging Assessments. Clin Genitourin Cancer. 2016; 14(1):e25–36. [PubMed: 26422014]
37. Israel GM, Bosniak MA. How I do it: evaluating renal masses. Radiology. 2005; 236(2):441–450. [PubMed: 16040900]
38. Pedrosa I, Alsop DC, Rofsky NM. Magnetic resonance imaging as a biomarker in renal cell carcinoma. Cancer. 2009; 115(10 Suppl):2334–2345. [PubMed: 19402070]
39. Khatri G, Pedrosa IM. 3T MR imaging protocol for characterization of renal masses. Applied Radiology. 2012; 41(SUPPL):22–26.
40. Butler BP, Novick AC, Miller DP, Campbell SA, Licht MR. Management of small unilateral renal cell carcinomas: radical versus nephron-sparing surgery. Urology. 1995; 45(1):34–40. discussion 40–31. [PubMed: 7817478]
41. Lerner SE, Hawkins CA, Blute ML, et al. Disease outcome in patients with low stage renal cell carcinoma treated with nephron sparing or radical surgery. J Urol. 1996; 155(6):1868–1873. [PubMed: 8618276]
42. Chawla SN, Crispen PL, Hanlon AL, Greenberg RE, Chen DY, Uzzo RG. The natural history of observed enhancing renal masses: meta-analysis and review of the world literature. J Urol. 2006; 175(2):425–431. [PubMed: 16406965]
43. Rosales JC, Haramis G, Moreno J, et al. Active surveillance for renal cortical neoplasms. J Urol. 2010; 183(5):1698–1702. [PubMed: 20299038]
44. Halverson SJ, Kunju LP, Bhalla R, et al. Accuracy of determining small renal mass management with risk stratified biopsies: confirmation by final pathology. J Urol. 2013; 189(2):441–446. [PubMed: 23253955]
45. Harvey CJ, Alsafi A, Kuzmich S, et al. Role of US Contrast Agents in the Assessment of Indeterminate Solid and Cystic Lesions in Native and Transplant Kidneys. Radiographics. 2015; 35(5):1419–1430. [PubMed: 26273994]
46. Yamashita Y, Takahashi M, Watanabe O, et al. Small renal cell carcinoma: pathologic and radiologic correlation. Radiology. 1992; 184(2):493–498. [PubMed: 1620854]
47. Forman HP, Middleton WD, Melson GL, McClennan BL. Hyperechoic renal cell carcinomas: increase in detection at US. Radiology. 1993; 188(2):431–434. [PubMed: 8327692]
48. Sidhar K, McGahan JP, Early HM, Corwin M, Fananapazir G, Gerscovich EO. Renal Cell Carcinomas: Sonographic Appearance Depending on Size and Histologic Type. J Ultrasound Med. 2016; 35(2):311–320. [PubMed: 26740493]
49. Barr RG, Peterson C, Hindi A. Evaluation of indeterminate renal masses with contrast-enhanced US: a diagnostic performance study. Radiology. 2014; 271(1):133–142. [PubMed: 24475802]
50. Bosniak MA, Megibow AJ, Hulnick DH, Horii S, Raghavendra BN. CT diagnosis of renal angiomyolipoma: the importance of detecting small amounts of fat. AJR Am J Roentgenol. 1988; 151(3):497–501. [PubMed: 3044036]
51. Simpson E, Patel U. Diagnosis of angiomyolipoma using computed tomography-region of interest < or =−10 HU or 4 adjacent pixels < or =−10 HU are recommended as the diagnostic thresholds. Clin Radiol. 2006; 61(5):410–416. [PubMed: 16679114]
52. Davenport MS, Neville AM, Ellis JH, Cohan RH, Chaudhry HS, Leder RA. Diagnosis of renal angiomyolipoma with hounsfield unit thresholds: effect of size of region of interest and nephrographic phase imaging. Radiology. 2011; 260(1):158–165. [PubMed: 21555349]
53. Wang Y, Li D, Haacke EM, Brown JJ. A three-point Dixon method for water and fat separation using 2D and 3D gradient-echo techniques. J Magn Reson Imaging. 1998; 8(3):703–710. [PubMed: 9626890]
54. Israel GM, Hindman N, Hecht E, Krinsky G. The use of opposed-phase chemical shift MRI in the diagnosis of renal angiomyolipomas. AJR Am J Roentgenol. 2005; 184(6):1868–1872. [PubMed: 15908544]

55. Jinzaki M, Tanimoto A, Narimatsu Y, et al. Angiomyolipoma: imaging findings in lesions with minimal fat. Radiology. 1997; 205(2):497–502. [PubMed: 9356635]
56. Outwater EK, Bhatia M, Siegelman ES, Burke MA, Mitchell DG. Lipid in renal clear cell carcinoma: detection on opposed-phase gradient-echo MR images. Radiology. 1997; 205(1):103–107. [PubMed: 9314970]
57. Pedrosa I, Chou MT, Ngo L, et al. MR classification of renal masses with pathologic correlation. Eur Radiol. 2008; 18(2):365–375. [PubMed: 17899106]
58. Hindman N, Ngo L, Genega EM, et al. Angiomyolipoma with minimal fat: can it be differentiated from clear cell renal cell carcinoma by using standard MR techniques? Radiology. 2012; 265(2): 468–477. [PubMed: 23012463]
59. Sasiwimonphan K, Takahashi N, Leibovich BC, Carter RE, Atwell TD, Kawashima A. Small (<4 cm) renal mass: differentiation of angiomyolipoma without visible fat from renal cell carcinoma utilizing MR imaging. Radiology. 2012; 263(1):160–168. [PubMed: 22344404]
60. Schieda N, Dilauro M, Moosavi B, et al. MRI evaluation of small (<4cm) solid renal masses: multivariate modeling improves diagnostic accuracy for angiomyolipoma without visible fat compared to univariate analysis. Eur Radiol. 2015
61. Lassel EA, Rao R, Schwenke C, Schoenberg SO, Michaely HJ. Diffusion-weighted imaging of focal renal lesions: a meta-analysis. Eur Radiol. 2014; 24(1):241–249. [PubMed: 24337912]
62. Kim JI, Cho JY, Moon KC, Lee HJ, Kim SH. Segmental enhancement inversion at biphasic multidetector CT: characteristic finding of small renal oncocytoma. Radiology. 2009; 252(2):441–448. [PubMed: 19508984]
63. Rosenkrantz AB, Hindman N, Fitzgerald EF, Niver BE, Melamed J, Babb JS. MRI features of renal oncocytoma and chromophobe renal cell carcinoma. AJR Am J Roentgenol. 2010; 195(6):W421–427. [PubMed: 21098174]
64. Lanzman RS, Robson PM, Sun MR, et al. Arterial spin-labeling MR imaging of renal masses: correlation with histopathologic findings. Radiology. 2012; 265(3):799–808. [PubMed: 23047841]
65. Tamai H, Takiguchi Y, Oka M, et al. Contrast-enhanced ultrasonography in the diagnosis of solid renal tumors. J Ultrasound Med. 2005; 24(12):1635–1640. [PubMed: 16301719]
66. Sheir KZ, El-Azab M, Mosbah A, El-Baz M, Shaaban AA. Differentiation of renal cell carcinoma subtypes by multislice computerized tomography. J Urol. 2005; 174(2):451–455. discussion 455. [PubMed: 16006863]
67. Kim JK, Kim TK, Ahn HJ, Kim CS, Kim KR, Cho KS. Differentiation of subtypes of renal cell carcinoma on helical CT scans. AJR Am J Roentgenol. 2002; 178(6):1499–1506. [PubMed: 12034628]
68. Sureka B, Lal A, Khandelwal N, et al. Dynamic computed tomography and Doppler findings in different subtypes of renal cell carcinoma with their histopathological correlation. J Cancer Res Ther. 2014; 10(3):552–557. [PubMed: 25313738]
69. Herts BR, Coll DM, Novick AC, et al. Enhancement characteristics of papillary renal neoplasms revealed on triphasic helical CT of the kidneys. AJR Am J Roentgenol. 2002; 178(2):367–372. [PubMed: 11804895]
70. Bata P, Gyebnar J, Tarnoki DL, et al. Clear cell renal cell carcinoma and papillary renal cell carcinoma: differentiation of distinct histological types with multiphase CT. Diagn Interv Radiol. 2013; 19(5):387–392. [PubMed: 23864331]
71. Oliva MR, Glickman JN, Zou KH, et al. Renal cell carcinoma: T1 and T2 signal intensity characteristics of papillary and clear cell types correlated with pathology. AJR Am J Roentgenol. 2009; 192(6):1524–1530. [PubMed: 19457814]
72. Roy C, Sauer B, Lindner V, Lang H, Saussine C, Jacqmin D. MR imaging of papillary renal neoplasms: potential application for characterization of small renal masses. European Radiology. 2007; 17(1):193–200. [PubMed: 16758161]
73. Pignot G, Elie C, Conquy S, et al. Survival analysis of 130 patients with papillary renal cell carcinoma: prognostic utility of type 1 and type 2 subclassification. Urology. 2007; 69(2):230–235. [PubMed: 17275070]

74. Rosenkrantz AB, Sekhar A, Genega EM, et al. Prognostic implications of the magnetic resonance imaging appearance in papillary renal cell carcinoma. Eur Radiol. 2013; 23(2):579–587. [PubMed: 22903703]

75. Yamada T, Endo M, Tsuboi M, et al. Differentiation of pathologic subtypes of papillary renal cell carcinoma on CT. AJR Am J Roentgenol. 2008; 191(5):1559–1563. [PubMed: 18941101]

76. Sun MR, Ngo L, Genega EM, et al. Renal cell carcinoma: dynamic contrast-enhanced MR imaging for differentiation of tumor subtypes--correlation with pathologic findings. Radiology. 2009; 250(3):793–802. [PubMed: 19244046]

77. Kang SK, Zhang A, Pandharipande PV, Chandarana H, Braithwaite RS, Littenberg B. DWI for Renal Mass Characterization: Systematic Review and Meta-Analysis of Diagnostic Test Performance. AJR Am J Roentgenol. 2015; 205(2):317–324. [PubMed: 26204281]

78. Vasudevan A, Davies RJ, Shannon BA, Cohen RJ. Incidental renal tumours: the frequency of benign lesions and the role of preoperative core biopsy. BJU Int. 2006; 97(5):946–949. [PubMed: 16643475]

79. Caoili EM, Bude RO, Higgins EJ, Hoff DL, Nghiem HV. Evaluation of sonographically guided percutaneous core biopsy of renal masses. AJR Am J Roentgenol. 2002; 179(2):373–378. [PubMed: 12130435]

80. Leveridge MJ, Finelli A, Kachura JR, et al. Outcomes of small renal mass needle core biopsy, nondiagnostic percutaneous biopsy, and the role of repeat biopsy. Eur Urol. 2011; 60(3):578–584. [PubMed: 21704449]

81. Wang R, Wolf JS Jr, Wood DP Jr, Higgins EJ, Hafez KS. Accuracy of percutaneous core biopsy in management of small renal masses. Urology. 2009; 73(3):586–590. discussion 590–581. [PubMed: 19118884]

Key Points

- Solid renal masses are a common manifestation of various types of renal pathology, which includes benign and malignant causes
- Lesion characterization is achievable in a great number of cases, with the use of state-of-the-art imaging techniques and evidence-based interpretation criteria
- Patient outcomes will potentially improve with advancements in diagnostic specificity of imaging methods

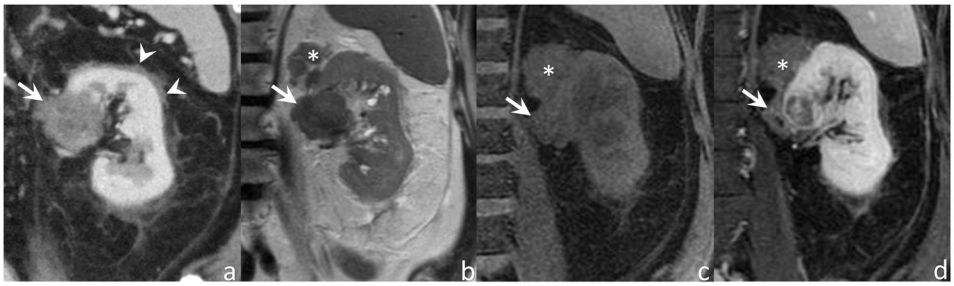

Fig. 1.

A 69-year-old man with diffuse large B-cell of the left kidney. Coronal contrast-enhanced CT image (A) showing a solid infiltrative lesion in the perihilar region of the left kidney (arrow). Note the perinephric soft tissue component surrounding the renal capsule (white arrowheads). Coronal single-shot fast spin-echo T2-weighted MR image (B) shows low-intermediate signal intensity in the mass, with interval development of new perinephric nodules (asterisk) compared with the prior CT (A). Coronal three-dimensional (3D) fat-saturated Dixon T1-weighted MR images before (C) and after (D) administration of contrast show heterogeneous enhancement of the lesion (arrows), with low-level homogeneous enhancement of the perirenal component (asterisks).

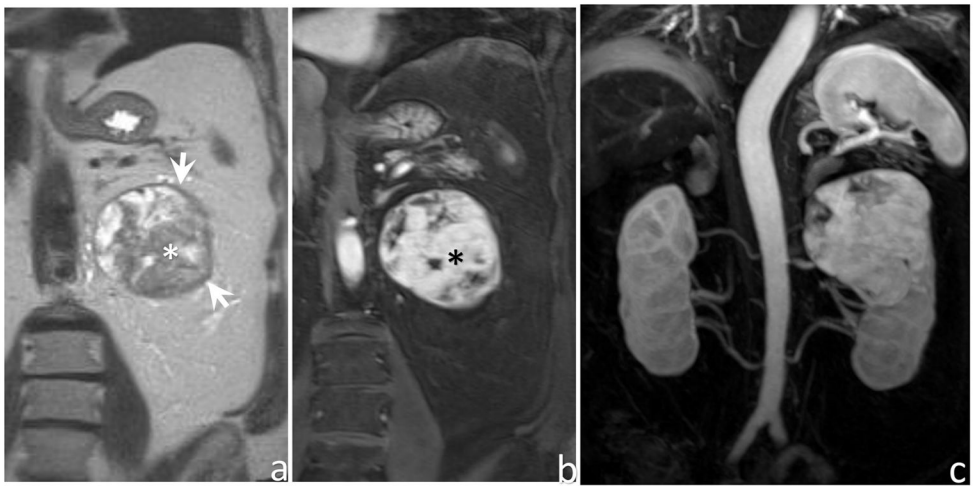

Fig. 2.

A 75-year-old man with oncocytoma. Coronal single-shot fast spin-echo T2-weighted MR image (A) shows a large mass in the left kidney (white arrows) with foci of high signal intensity in the periphery and central areas of intermediate signal intensity. Note that the central component (asterisk) shows avid postcontrast enhancement on the fat-saturated Dixon-based T1-weighted gradient echo acquisition during the corticomedullary phase (B). Maximum intensity projection of postcontrast T1-weighted Dixon-based acquisition (C) shows invasion of the renal hilum fat, which was confirmed after nephrectomy.

Fig. 3.

A 47-year-old woman with angiomyolipoma in the left kidney. Coronal (A) and axial (B) non–contrastenhanced CT images show an 8-cm circumscribed mass in the left upper pole (arrows), predominantly composed of low-attenuation elements (bulk fat), similar to that of retroperitoneal and subcutaneous fat (asterisks). Also note some streaks of soft tissue within the lesion, corresponding with vascular and smooth muscle components (arrowheads).

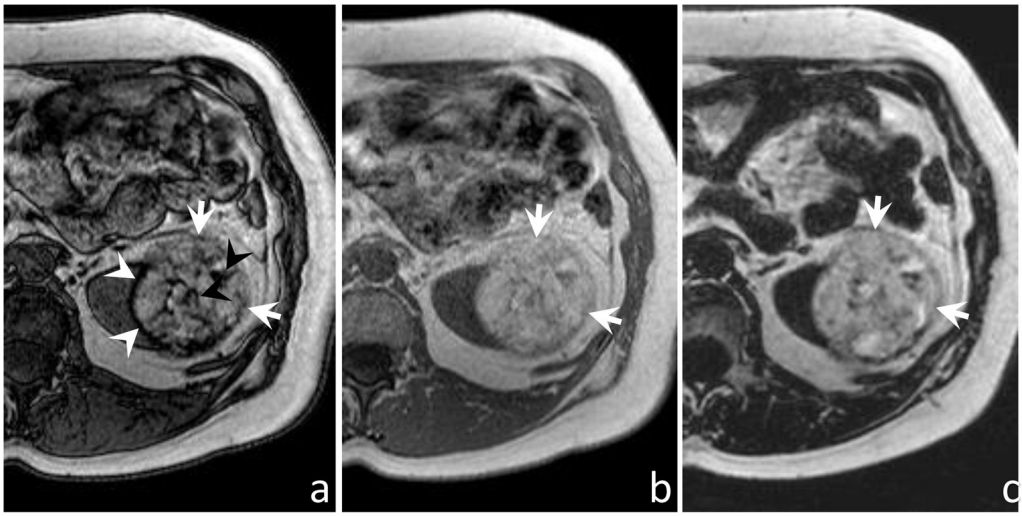

Fig. 4.

A 47-year-old woman with angiomyolipoma in the left kidney (same patient from previous figure). Opposed-phase (A), in-phase (B), and fat-only (C) reconstructions from an axial T1-weighted Dixon acquisition. The circumscribed mass (arrows) shows high signal intensity on all images, following the same pattern of retroperitoneal and subcutaneous fat. On opposed-phase images, note the signal dropout at the interface between the mass and the kidney (white arrowheads), also known as India-ink artifact. Signal dropout in areas within the mass (black arrowheads) indicate coexistence of fat and nonfat elements (ie, intravoxel fat).

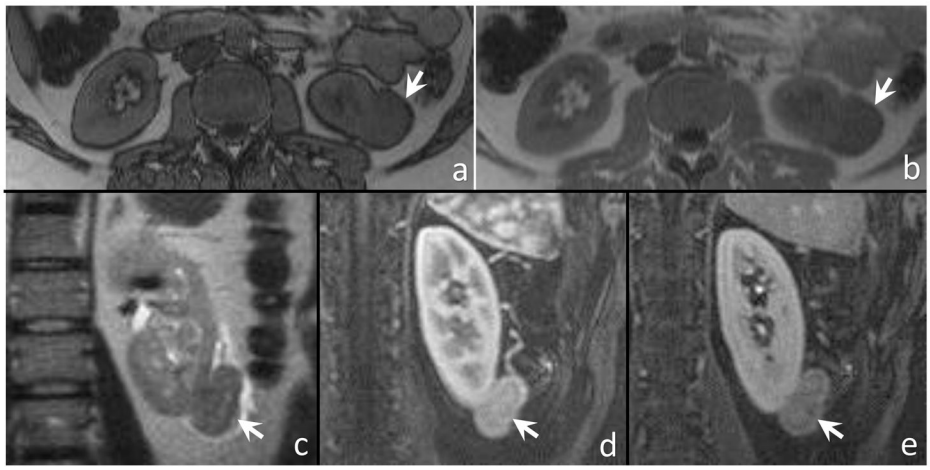

Fig. 5.

A 40-year-old woman with minimal-fat angiomyolipoma in the left kidney. Axial gradient recalled echo (GRE) T1-weighted opposed-phase (A) and in-phase (B) MR images show a slightly hypointense circumscribed lesion in the lower pole of the left kidney (arrows), without significant signal dropout to suggest intravoxel fat. Coronal non–fat-saturated single-shot fast spin-echo T2-weighted MR image (C) shows homogeneous hypo-intense signal in the lesion (arrow). Dynamic contrast-enhanced fat-saturated spoiled gradient recalled (SPGR) T1-weighted MR images during corticomedullary (D) and excretory (E) phases show avid early enhancement of the lesion and subsequent washout (arrows).

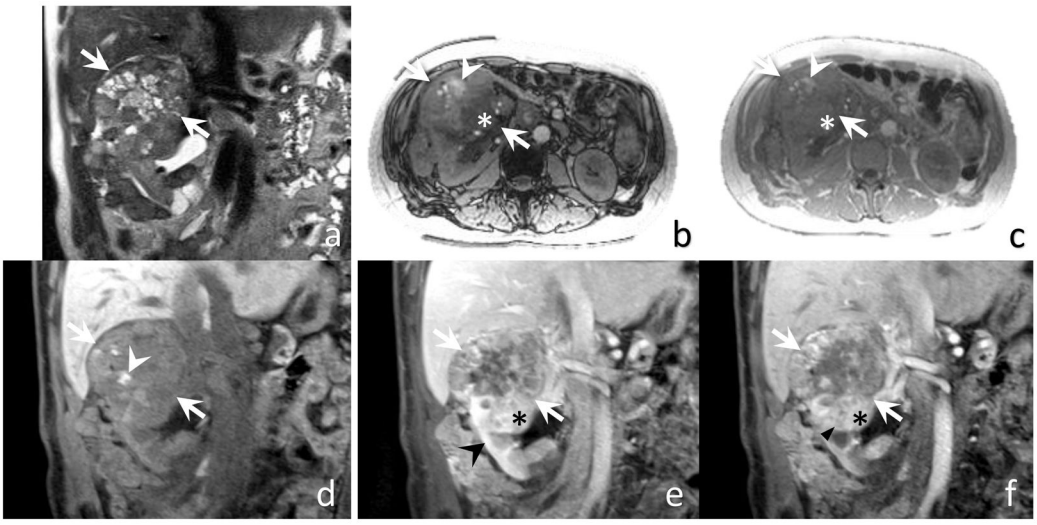

Fig. 6.

A 55-year-old man with clear cell renal cell carcinoma in the right kidney. Coronal single-shot fast spinecho T2-weighted MR image (A) shows an infiltrative mass (arrows) with heterogeneous and predominantly high signal intensity in the right upper pole. Area of signal dropout (asterisk) is identified in the T1-weighted opposed-phase image (B) compared with the IP image (C), consistent with intravoxel fat. There are also foci of high signal intensity (white arrowheads), related to hemorrhage, better seen on the precontrast fat-saturated T1-weighted SPGR acquisition (D). Postcontrast images using the same acquisition as in D, during the corticomedullary (E) and nephrographic (F) phases, show heterogeneous enhancement in the mass (arrows) with areas of avid enhancement (asterisk), similar to that of normal renal cortex (black arrowhead).

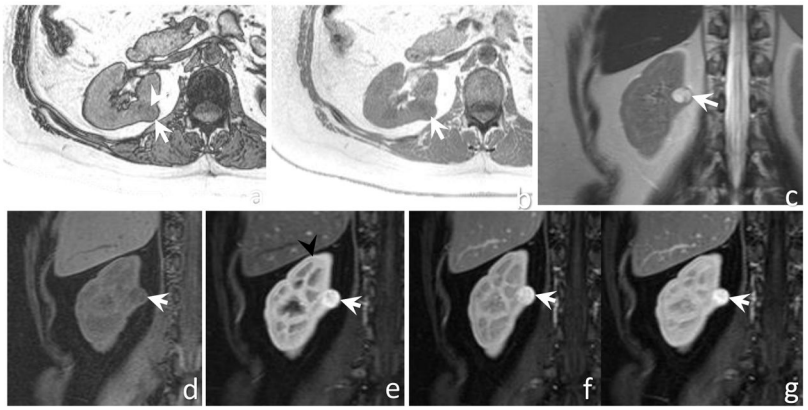

Fig. 7.

A 40-year-old woman with clear cell renal cell carcinoma in the right kidney (arrows). Axial GRE T1-weighted opposed-phase (A) and in-phase (B) MR images show mild signal dropout within the mass (arrowhead), consistent with intravoxel fat. There is marked hyperintense signal on coronal single-shot fast spin-echo T2- weighted MR images (C). Note the early and avid enhancement on dynamic postcontrast images (E–G; precontrast, D), higher than that of normal renal cortex.

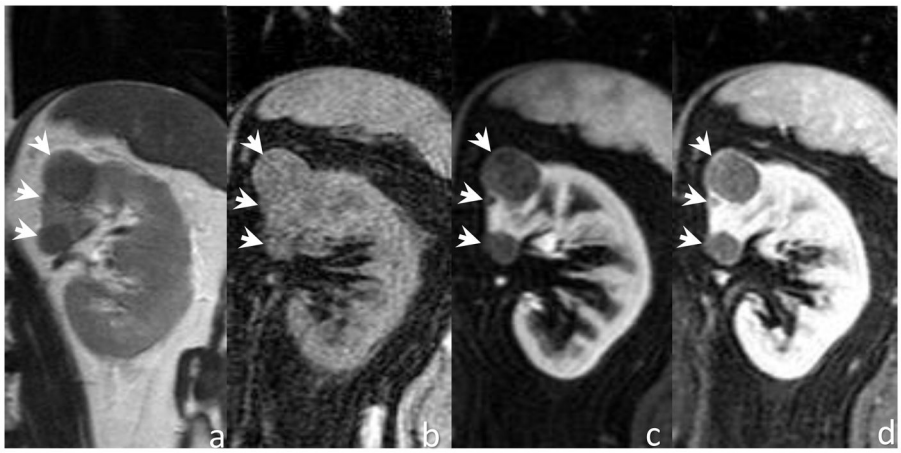

Fig. 8.

65-year-old male with multifocal papillary RCC. Coronal single-shot fast spin-echo T2-weighted MR image demonstrates three circumscribed lesions with homogeneous hypointense signal in the perihilar and upper pole of the left kidney. Coronal 3D fat-saturated Dixon T1-weighted MR images before (b) and after-contrast during the corticomedullary (c) and nephrographic (d) phases show low-level homogeneous progressive enhancement.

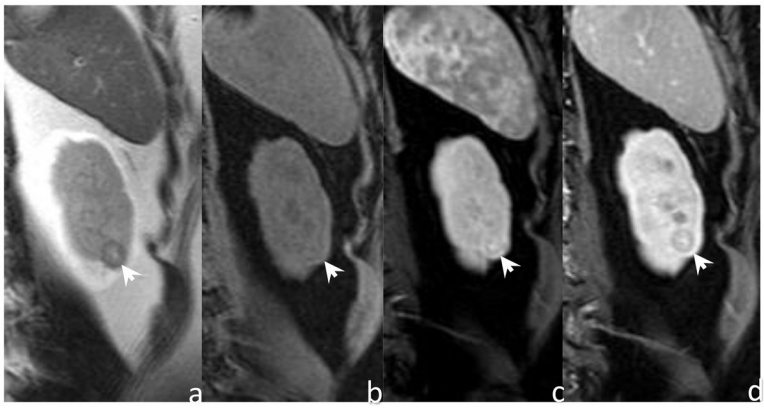

Fig. 9.

A 42-year-old woman with chromophobe RCC in the left kidney (arrows). Coronal single-shot fast spinecho T2-weighted MR image (A) shows a 1.3-cm, slightly heterogeneous, predominantly hypointense lesion in the left lower pole. Fat-saturated 3D Dixon T1-weighted MR image shows moderate enhancement of the lesion on the corticomedullary (C) and nephrographic (D) phases compared with precontrast (B).

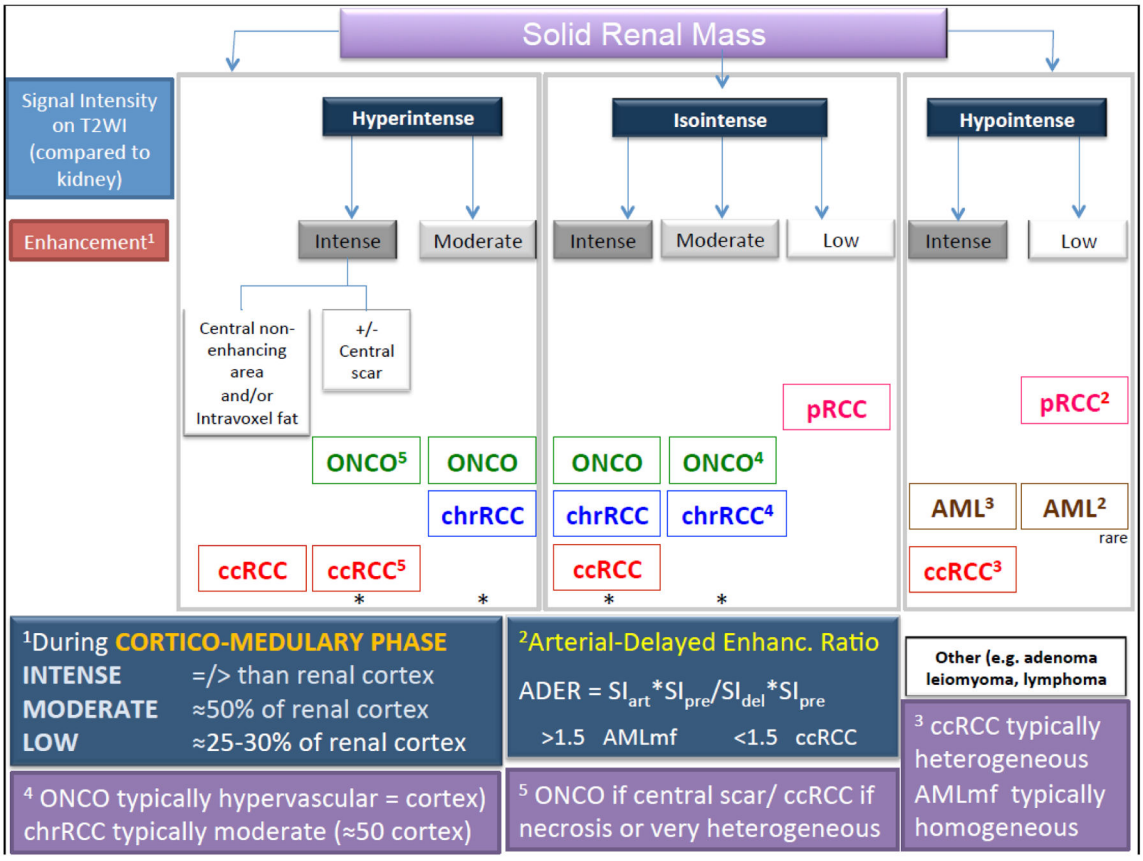

Fig. 10.

Diagnostic algorithm for characterization of solid renal masses. a Enhancement during corticomedullary phase: Intense, greater than or equal to renal cortex; moderate, approximately 50% of renal cortex; mild, approximately 25% to 30% of renal cortex. b Arterial-delayed enhancement ratio (ADER), which is the difference in signal intensity between arterial and precontrast phase divided by the difference between delayed and precontrast phase. ADER greater than 1.5 favors minimal-fat AML, whereas less than 1.5 favors ccRCC. ccRCC is typically heterogeneous; minimal-fat AML is typically homogeneous. d Oncocytoma (ONCO) is more commonly hypervascular (enhances similarly to renal cortex), whereas chrRCC has typically moderate enhancement (approximately 50% of renal cortex). e Oncocytoma if central scar, whereas ccRCC is more likely if necrosis is present or if tumor is heterogeneous. Asterisks mean that ancillary findings should be used for characterization. T2WI, T2-weighted imaging.

Table 1

Multidetector contrast-enhanced computed tomography protocol for renal mass characterization

Renal Mass Multidetector CT Protocol				
Phases	**Noncontrast**	**Corticomedullary**[a]	**Nephrographic**	**Delayed**
Phase timing	—	40 s	100–120 s	5–7 min
Coverage	Kidneys	Diaphragm through kidneys	Diaphragm through kidneys	Kidneys
FOV	Whole body	Whole body	Whole body	Whole body
Reconstructions	Axial: 3 mm	Axial: 3 mm Coronal: 2 mm Sagittal: 2 mm	Axial: 3 mm Coronal: 2 mm Sagittal: 2 mm	Axial: 3 mm Coronal: 2 mm Sagittal: 2 mm

Intravenous contrast: 100 to 150 mL of low-osmolar iodinated contrast at 5 mL/s.

Abbreviation: FOV, field of view.

[a]Optional.

Table 2

Contrast-enhanced 3T MR imaging protocol for renal mass characterization

Renal Mass MR Protocol (3T)							
Acquisition	**TR (ms)**	**TE (ms)**	**Flip Angle (Degrees)**	**Bandwidth (Hz/Pixel)**	**Slice Thickness/Gap**	**FOV (cm)**	**Matrix**
Coronal T2-weighted SSFSE	960	80	90	652	5/1	40 × 45	312 × 279
Axial T2-weighted fat-saturated SSFSE	920	80	90	543	5/1	40 × 30	304 × 168
Axial 2D T1-weighted GRE IP/OP	120	2.3/1.15	55	1215	5/1	40 × 38	400 × 269
Axial DWI	1060	53	90	36.5	7/1	44 × 35	144 × 115
Sagittal oblique 3D Dixon (kidneys)[a]	3.7	1.32/2.3	10	1568	3/–1.5	30 × 30	248 × 230
Coronal 3D Dixon[b]	3.8	1.7/2.1	10	1923	3/–1.5	39 × 40	260 × 223
Axial 3D Dixon	2.2	1.16/2.1	10	1852	3/–1.5	38 × 33	252 × 218

Intravenous contrast: 0.1 mmol/kg gadolinium chelate at 2 mL/s, followed by 20-mL saline flush.

Abbreviations: 2D, two dimensional; 3D, three dimensional; GRE, gradient recalled echo; IP, in phase; OP, opposed-phased; SSFSE, single-shot fast spin echo; TE, echo time; TR, repetition time.

[a] Precontrast and postcontrast (3 minutes).

[b] Before, bolus-tracking (left ventricle enhancement), early arterial (ask for 2 breath in/breath out, then hold), cortico-medullary (40 seconds), nephrographic (90 seconds).

Radiol Clin North Am. Author manuscript; available in PMC 2017 September 21.